



ELSEVIER

Available online at www.sciencedirect.com

Infrared multiphoton microscopy: subcellular-resolved deep tissue imaging

Volker Andresen^{1,2}, Stephanie Alexander¹, Wolfgang-Moritz Heupel¹, Markus Hirschberg¹, Robert M Hoffman³ and Peter Friedl^{1,4}

Multiphoton microscopy (MPM) is the method of choice for investigating cells and cellular functions in deep tissue sections and organs. Here we present the setup and applications of infrared-(IR-)MPM using excitation wavelengths above 1080 nm. IR-MPM enables the use of red fluorophores and fluorescent proteins, doubles imaging depth, improves second harmonic generation of tissue structures, and strongly reduces phototoxicity and photobleaching, compared with conventional MPM. Furthermore, it still provides subcellular resolution at depths of several hundred micrometers and thus will enhance long-term live cell and deep tissue microscopy.

Addresses

¹ University of Würzburg, Rudolf-Virchow Center for Experimental Biomedicine and Department of Dermatology, Venerology, and Allergology, Josef-Schneider-Strasse 2, 97080 Würzburg, Germany

² LaVision BioTec GmbH, Meisenstrasse 65, 33607 Bielefeld, Germany

³ AntiCancer, Inc., 7917 Ostrow Street, San Diego, CA 92111 and Department of Surgery, University of California, San Diego, 200 West Arbor Drive, San Diego, CA 92103-8220, USA

⁴ Microscopical Imaging Centre, Department of Cell Biology, Nijmegen Center for Molecular Life Science, Radboud University Nijmegen Medical Centre, P.O. 9101, 6500 HB, Nijmegen, The Netherlands

Corresponding author: Friedl, Peter (P.Friedl@ncmls.ru.nl)

Current Opinion in Biotechnology 2009, **20**:1–9

This review comes from a themed issue on Analytical biotechnology Edited by Christopher Contag and Kevin Eliceiri.

0958-1669/\$ – see front matter © 2009 Elsevier Ltd. All rights reserved.

DOI [10.1016/j.copbio.2009.02.008](https://doi.org/10.1016/j.copbio.2009.02.008)

Introduction

Multiphoton microscopy (MPM) has emerged as a significant measurement method for intravital and live cell studies in neuroscience, immunology, and cancer research. The main advantage of MPM over other imaging approaches is its ability to observe cell migration, cell–cell interaction, and intracellular signalling deeply inside dense tissues and organs in live animals [1–3]. Compared with confocal laser-scanning microscopy, MPM substantially increases the maximum imaging depth from a few 10 μm up to nearly 1 mm in certain types of tissues, such as brain [4]. Further advantages over confocal microscopy are an inherent submicron spatial resolution that still allows

revelation of subcellular details and fine tissue structures; reduced scattering and absorption due to longer excitation wavelengths and significantly reduced phototoxicity and photobleaching in out-of-focus regions [5]. In addition MPM enables excitation of the characteristic UV absorption bands of endogenous fluorophores and second harmonic generation (SHG) of anisotropic biological structures like collagen and skeletal muscle fibers that possess large hyperpolarizabilities [6–8]. All other currently available optical imaging techniques either lack the capability to image deeply in scattering tissue or lack submicron spatial resolution.

Despite these advantages multiphoton excitation also comprises significant limitations: the still insufficient penetration depth in optically dense samples including connective tissue and cell-rich tissues such as skin [9], lymph node [10], muscle [11], kidney [12], and tumors [13]; the decrease in spatial resolution with increasing depth in tissues caused by light scattering and distortion of the beam profile [14^{*}]; the light-induced toxicity toward sensitive cell functions; and the inefficient excitation of red and near-infrared (NIR) fluorophores. The latter is of particular importance as many red-shifted fluorophores have become standard sensors for transcutaneous detection of deep tissue lesions in live animals, including whole-body imaging [15]. A common approach to compensate for inefficient fluorophore excitation is to increase the laser power above the non-toxic level. However, once a certain power level is crossed the nonlinear photodamage rises faster with increasing laser power than the number of excited molecules [16^{**}] and, therefore, strongly increases phototoxic damage to sensitive cell and tissue functions, such as cell migration and signalling [17].

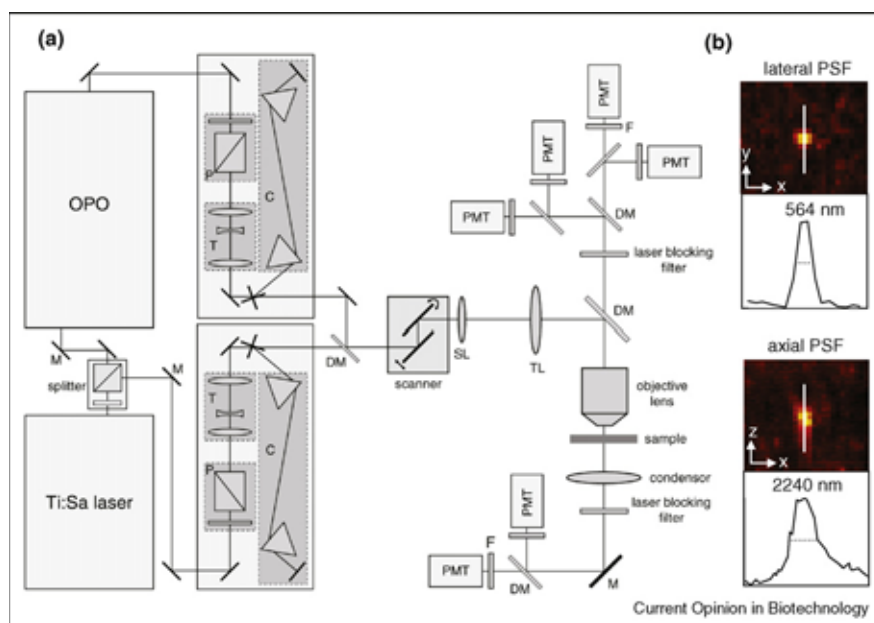
To overcome some of the present drawbacks of NIR-MPM, particularly limited tissue penetration, light-induced cell damage, and poor excitation of red fluorophores, we describe here the setup and life science applications of IR-MPM with reference to live cell and deep tissue imaging in skin, lymph nodes, and cancer lesions.

Infrared-excited MPM: system design

By using an optical parametric oscillator (OPO) as infrared multiphoton light source we extend multiphoton and second harmonic generation (SHG) microscopy toward red wavelengths. A high-repetition short-pulsed Ti:Sa

2 Analytical biotechnology

Figure 1



Setup and spatial resolution of an intravital NIR and IR multiphoton microscope. **(a)** The beam of a mode-locked Ti:Sa laser (775 or 830 nm; 80 MHz; 120 fs) is split up (90/10%) to pump an optical parametric oscillator (OPO) and to directly excite the sample. The OPO allows automated, software-controlled wavelength tuning as well as output power stabilization through the use of an integrated spectrometer in combination with motorized cavity length tuning and a motorized cavity end mirror. Both NIR and IR beams pass independent beam-shaping devices that each consist of a pair of crossed polarizers (P) for controlling the excitation power, a telescope (T) for adapting the beam diameter to the size of the objective lens back focal plane, and a chirp compensation arrangement (C) that compensates for pulse broadening caused by the intermediate optics and the objective lens. Using the latter pulse lengths are reduced from ~ 380 to ~ 120 fs (Ti:Sa) and from ~ 270 fs to ~ 180 fs (OPO) at the egression of the objective lens (V Andresen, P Friedl, unpublished data). To achieve maximum efficiency all optical elements in the OPO pathway are coated and corrected for the extended wavelength area. Both beams are uniaxially combined via a dichromatic mirror (DM; slope at 1020 nm) and jointly passed onto a pair of galvanometric scanners. Emission signals are collected in forward direction by a special condenser with 1.4 NA and in backward direction through the objective lens. Spectral separation is achieved by dichromatic mirrors and bandpass filters in front of each photomultiplier (PMT). In forward and backward direction, the laser light is rejected by blocking filters. Abbreviations: SL, scan lens; TL, tube lens; M, mirror. **(b)** Lateral and axial point spread function (PSF) for IR-MPM. An IR $20\times$ objective lens with 0.95 NA and an excitation wavelength of 1100 nm was used to excite red fluorescent polystyrene beads (Molecular Probes) with a diameter below the resolution limit (100 nm). The power in the focus was 15 mW and the pixel dwell-time 240 μ s in order to collect enough signal. The dimensions of the PSF were calculated by applying one-dimensional Gaussian fits to the respective x, y, and z intensity profiles and taking the full width half maximum values. The resultant PSF represents an average of 15 independent beads at different positions within the field-of-view.

laser (Chameleon XR, Coherent) that generates radiation from 710 to 980 nm is, on one hand, used for direct excitation. On the other hand, it serves as synchronous pump-source for an OPO (PP Automatic, APE) that is based on non-critical phase-matched interaction within a periodically poled crystal (Figure 1a). Optical parametric oscillation is a nonlinear process that converts a short wavelength pump beam into two tuneable beams (signal and idler) of longer wavelengths [18]. For a pump wavelength of 775 or 830 nm, the OPO signal beam spectrum ranges from 1060 to 1450 nm.

Both beams pass independent beam-shaping devices that are used to control their diameters, collimations, pulse lengths, and powers and afterward enter a scan-head (TriM Scope, LaVision BioTec) optimized for simultaneous use of Ti:Sa and OPO radiation. By means of a dichromatic mirror the beams are uniaxially

combined and afterward jointly reflected by a pair of galvanometric scanners. The objective lens ($20\times$ IR, NA 0.95; Olympus) features a long working distance of 2 mm for deep tissue penetration, and it is coated and corrected for a wide wavelength range from 430 to 1450 nm.

System performance and simultaneous use of Ti:Sa and OPO radiation

To achieve simultaneous Ti:Sa and OPO excitation of the sample a beam splitter divides the Ti:Sa beam for pumping the OPO and direct imaging (Figure 1a). The split ratio is determined by the amount of light needed for adequate excitation, which in turn, depends on the characteristics of the sample (optical density, constituents, and fluorophore absorption cross-section) and the aspired imaging depth. In practice, a 90/10 splitting is useful for pumping the OPO and direct Ti:Sa imaging to

generate powers above 100 mW in the excitation foci of both beams at 830 nm and 1120 nm, respectively.

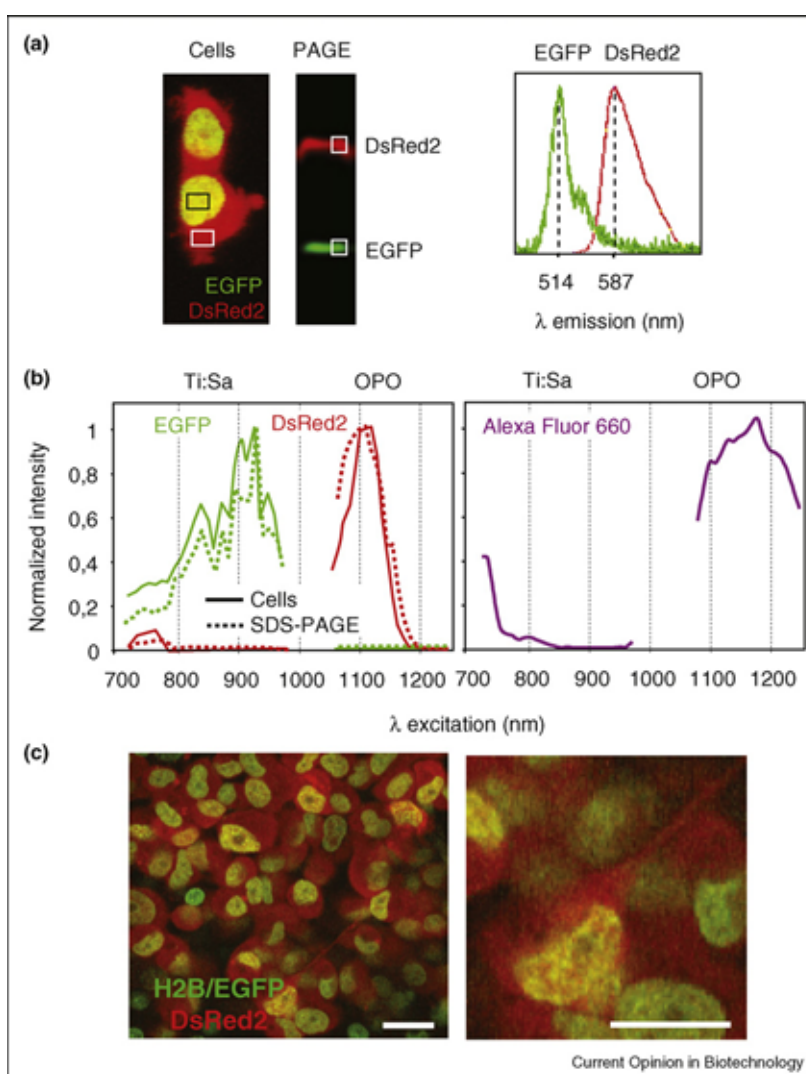
The optical resolution of the IR-MPM was quantified by measuring the lateral and axial point spread function (PSF) [19] using red fluorescent polystyrene beads (Molecular Probes). For a 20× IR objective lens with 0.95 NA and an excitation wavelength of 1100 nm, and water as immersion medium, the dimensions of the IR-MPM PSF amounted to 564 nm in lateral and 2240 nm in axial direction. These values are slightly above the expected theoretical numbers that is most probably due to a non-

perfect correction of the objective lens at the long excitation wavelengths and confirm previous data using excitation at 1500 nm and 120 fs pulse width [20]. Thus, IR-MPM is suited to provide near diffraction-limited images.

Two-photon excitation and emission spectra of red dyes and fluorescent proteins

In MPM fluorescent molecules or proteins are excited by simultaneous absorption of $n \geq 2$ photons that together provide the energy needed for excitation. This predicts optimum excitation wavelengths at roughly twice the corresponding single-photon wavelength [21]. Therefore,

Figure 2



NIR and IR 2-photon excitation and emission spectra. Excitation spectra were recorded by taking multiple images of a single sample plane at different Ti:Sa laser and OPO wavelengths and corrected for power density and bleaching between the scans. To acquire emission spectra of red and endogenous fluorophores and SHG the signals were collected by the objective lens, passed through a spectrograph and detected using a CCD camera. **(a)** HT-1080 cells expressing cytoplasmic DsRed2 and Histone-2B-EGFP [15] before and after SDS-PAGE under native conditions. The square boxes indicate the regions where the spectra were taken from. **(b)** 2-photon excitation spectra of EGFP, DsRed2, and Alexa Fluor 660. The solid lines represent the isolated protein in SDS-PAGE or soluble Alexa Fluor 660 and the dashed lines living dual-color cells. The calculated efficiency to excite DsRed2 at 1100 nm was 20-fold higher compared with excitation at 760 nm. **(c)** Simultaneous excitation of EGFP at 830 nm and DsRed2 at 1100 nm in live, non-fixed HT-1080 dual-color cells. Bars, 20 μm .

4 Analytical biotechnology

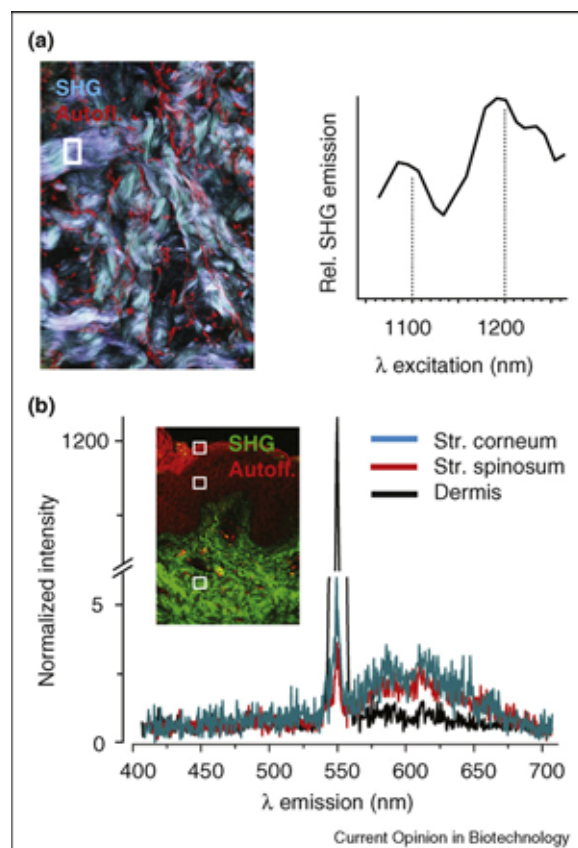
excitation efficiency of red fluorophores was supposed to significantly increase above 1100 nm.

The excitation and emission spectra of EGFP and DsRed2 were obtained from living dual-color human fibrosarcoma cells (HT-1080) [15] expressing both nuclear EGFP/Histone-2B (H2B) and cytoplasmic DsRed2 as well as the isolated proteins, extracted from the cells and electrophoretically separated (Figure 2a). The most efficient excitation of EGFP was at 930 nm, as reported [21], but no excitation was observed between 1060 and 1350 nm. By contrast, DsRed2 showed a small excitation peak at 760 nm and 20-fold higher efficiency from 1090 to 1120 nm (Figure 2b). Alexa Fluor 660 showed strong excitation between 1070 and 1300 nm with a peak at 1180 nm (Figure 2b).

When using two laser beams with different wavelengths for imaging, their focal volumes must overlap precisely. In lateral direction this is achieved by adjusting the tilt of one beam with respect to the other while imaging a reference structure that is excited by both beams simultaneously, such as SHG of criss-crossing collagen fibers. To match the focal positions in axial direction the telescope within the beam-shaping device of the OPO is used (Figure 1a, 'T'). While taking 3D-stacks of the transition of a coverslip to a homogeneous dye solution that is excited by both beams the telescope is adjusted until the slopes superimpose. Misalignment leads to ghost images that may, in addition, originate from different sample planes. Using simultaneous excitation of EGFP and DsRed2 in live dual-color HT-1080 cells, small ruffles and intranuclear structures were detected with excellent spatial resolution (Figure 2c), confirming the applicability of IR-MPM for high-resolution live cell imaging in tissue.

To simultaneously excite fluorescence and other specific signals like SHG emitted from tissue structures, optimal laser wavelengths for combined excitation were determined. Because SHG is a non-centrosymmetric process, the forward signal is four to eight times stronger compared with that generated in backward direction [6]; therefore, registration of fluorescence and SHG signals is achieved in backward and forward direction via the objective lens and a condenser, respectively. Fibrillar collagen exhibited narrow SHG bands from a broad input wavelength range with maxima at 1100 and 1180 nm (Figure 3a). Compared with NIR-generated SHG at fibrillar dermal collagen, the emission was 5–30-fold more intense using 1100 nm excitation (V Andresen, WM Heupel, P Friedl, unpublished data). The ratio of SHG to autofluorescent signals was approximately 500:1 (Figure 3b) that exceeds typical ratios obtained with Ti:Sa excitation. Thus, 1100 nm is a suitable OPO wavelength for simultaneous excitation of DsRed2, Alexa Fluor 660, and SHG of collagen-rich tissue.

Figure 3



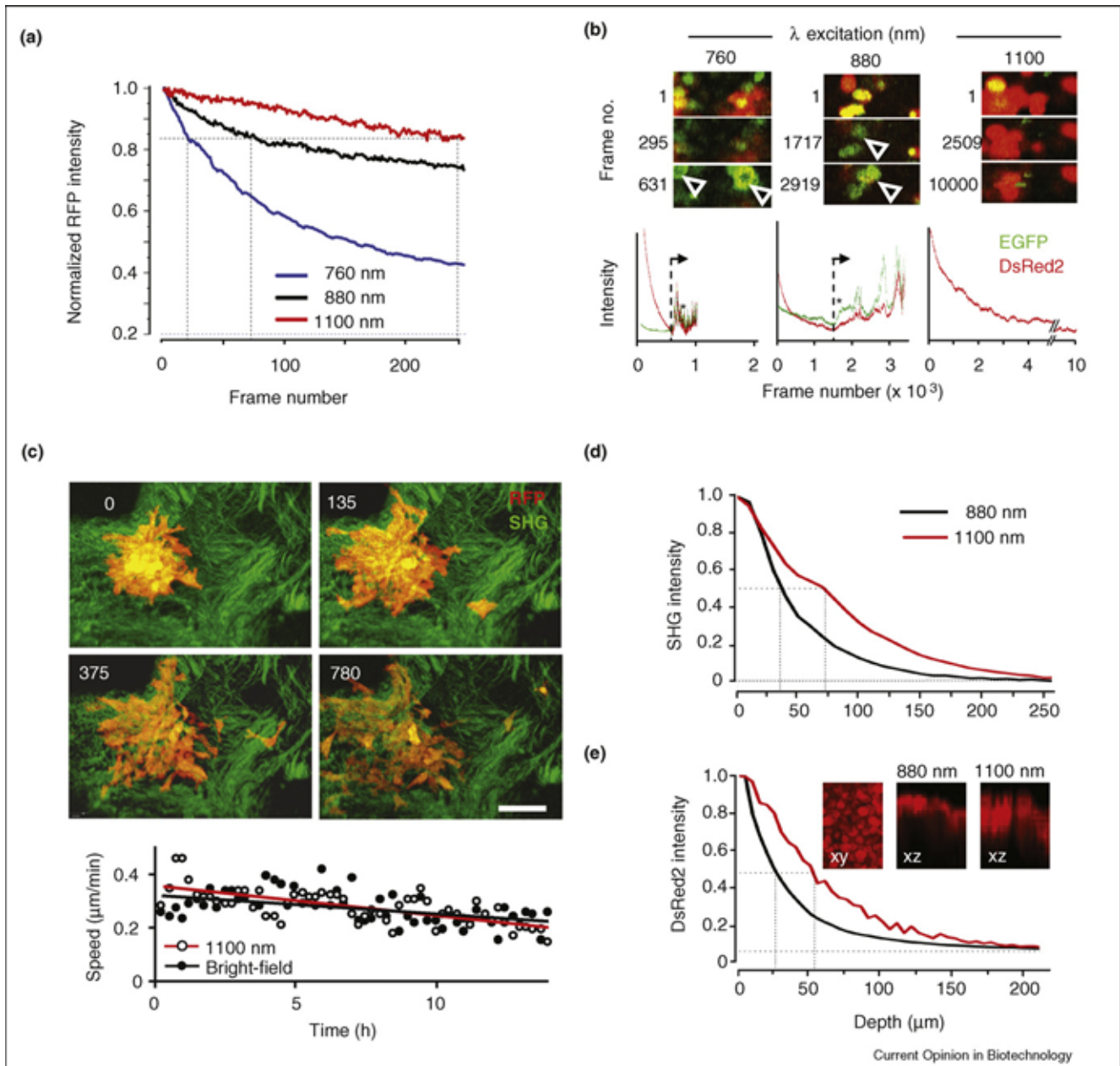
IR 2-photon generated second harmonic signal. (a) SHG spectra (right) from collagen-rich regions of native human dermis (left). Box, region of measurement. (b) Emission spectra at 1100 nm from human skin. The boxes indicate the regions in stratum corneum, epidermis, and dermis where the spectra were taken. The SHG peak for fibrillar collagen is at half of the excitation wavelength.

Photobleaching, photodamage, and tissue penetration

For live cell microscopy, repeated exposure to laser light leads to photobleaching of fluorophores associated with *de novo* formation of reactive oxygen intermediates and heat, ultimately compromising imaging sensitivity as well as cell viability and function [22[•]].

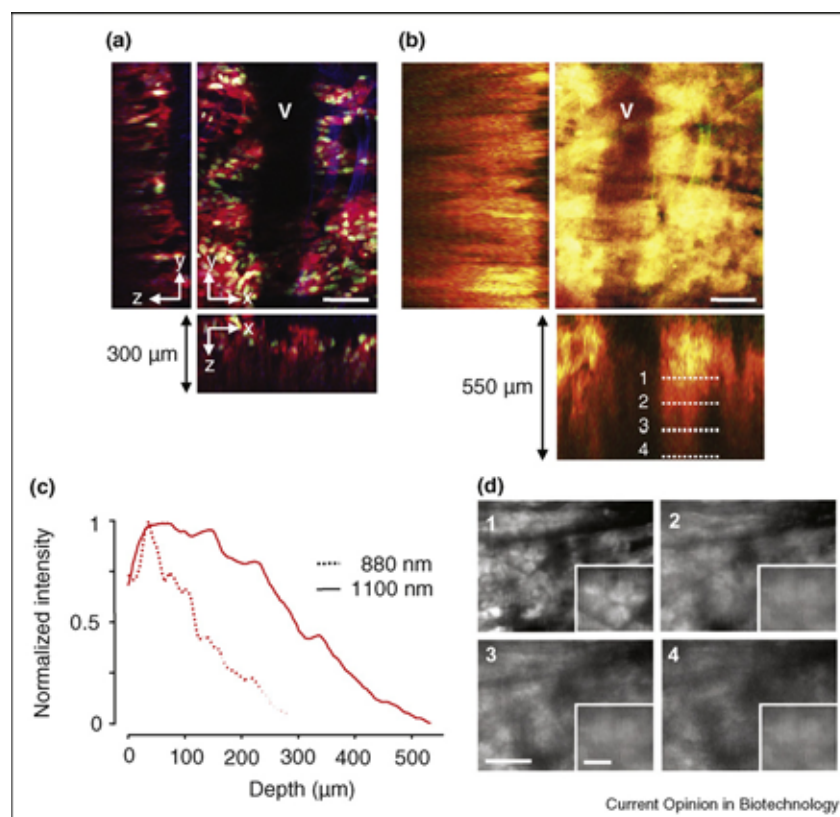
Photobleaching of DsRed2 in live cells at 1100 nm was 4 and 10 times lower compared with excitation at 880 and 760 nm, respectively (Figure 4a). At a high laser power of 117 mW, respective aggregation of EGFP and DsRed2 in live cells was reached after 500 and 1700 consecutive scans corresponding to 3 and 10 min continuous illumination time at 760 nm and 880 nm (Figure 4b). By contrast, no protein aggregation was detected after up to 10⁴ scans or 60 min of continuous exposure time using an excitation wavelength of 1100 nm (Figure 4b). To exclude non-structural, latent photodamage actin-driven cell migration was tested owing to its immediate energy dependency

Figure 4



Photobleaching, phototoxicity, and tissue penetration of IR-MPM. **(a)** Photobleaching of DsRed2 measured as decrease in emission during consecutive scanning at 760, 880, and 1100 nm excitation wavelengths and a power of 75 mW. The samples were subjected to 250 consecutive scans and the emission intensity was quantified as average pixel intensity of the entire scanning field and normalized to the intensity of the first frame. The dashed lines indicate the bleaching efficiency normalized to the end-point of the decay of emission intensity at 1100 nm. **(b)** Protein condensation due to continuous excitation. Continuous imaging of dual-color HT-1080 cells at a high excitation power (110 mW) and a frame rate of 2.8 fps. Arrowheads and asterisks indicate aggregates of condensed protein. **(c)** Undiminished emigration of HT-1080 cells from a multicellular spheroid on a dermis slice during continuous excitation at 1100 nm and 117 mW power in the focus. The numbers indicate the elapsed time (min). The population velocity obtained by cell tracking was compared to cells monitored by conventional bright-field microscopy. The near-completely overlapping regression curves of migration speed are shown. Penetration depth measurements for SHG **(d)** of 4 mm thick native human dermis slice and for fluorescence **(e)** of dual-color HT-1080 cell spheroid of 1 mm in diameter. For both, 3D dermis or multicellular spheroid, excitation of 880 and 1100 nm was used at an intensity of 75 mW and the respective SHG or fluorescence emission was collected at identical PMT sensitivity. Dashed lines in (d) and (e) indicate 50% emission signal intensity measured as normalized mean pixel intensity of the entire scanning field. Bar (c), 150 μm .

Figure 5



Deep IR 2-photon tissue microscopy of DsRed2-expressing tumor xenograft *in vivo*. 3D data stack of human dual-color xenograft of HT1080 fibrosarcoma cells implanted into the mouse dermis [25] using (a) 880 and (b) 1100 nm excitation at a power of 75 mW in the sample. Step-size in z-direction was 5 μm. V indicates a region with a large blood vessel (negative contrast). (c) Normalized fluorescence intensity for DsRed2 as a function of penetration depth. The initial slope of the intensity profile corresponds to the position of the lesion 10 to 50 μm below the dermis interface. (d) Decrease in spatial resolution with increasing penetration depth using 1100 nm excitation in the z-planes indicated by the dashed lines in (b). The insets show magnified details from the overview images. Bars indicate 100 μm (a) and (b), 50 μm (d), and 20 μm ((d), insets).

and sensitivity to physical or chemical assault. No signs of compromised migration or laser-induced toxicity including cell rounding, protein condensation, or loss of fluorescence were detected despite continuous sample exposure to 1100 nm radiation over 14 h (Figure 4c). Thus, IR-MPM shows very low levels of photobleaching and photodamage.

IR-MPM for deep tissue microscopy

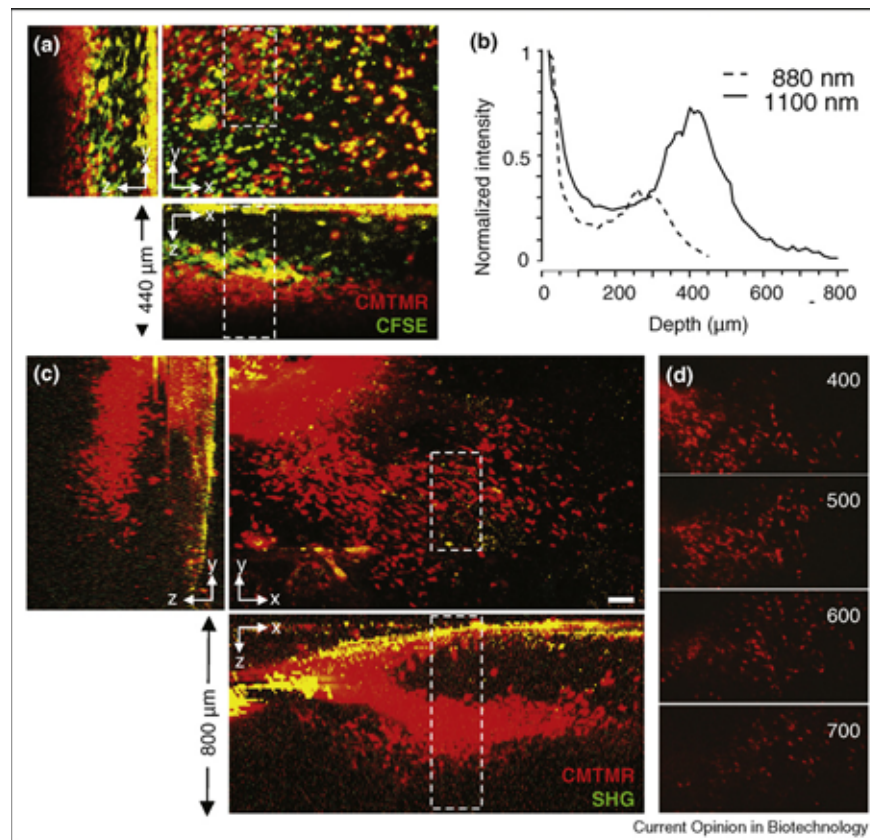
Whereas NIR radiation is in comparison to visible light poorly absorbed by water, the water absorption increases for excitation wavelengths above 900 nm [23], thus posing a potential limitation of IR-MPM for biomedical applications in live, hydrated tissues. Taking this into account, the maximum imaging depth for fibrillar collagen in native human dermis was increased twofold for SHG excitation at 1100 nm compared with 880 nm excitation (Figure 4d). Likewise, DsRed2 fluorescent cells in aqueous medium could be detected in two times deeper layers within a solid multicellular spheroid (Figure 4c). Thus, IR-MPM is

suited to image more deeply in biological tissues, as predicted [24].

Consequently, in thick xenografts of dual-color HT1080 cells, eight days after implantation into the mouse dermis [25], the detection of DsRed2 signal at 1100 nm was increased twofold reaching up to 500 μm tissue penetration, compared with excitation at 880 nm (Figure 5a–c). CMTMR-labeled dendritic cells in the lymph node were detected down to a depth of 700 μm from the upper cortex using 1100 nm excitation (Figure 6a–c).

Another severe limitation for deep tissue multiphoton microscopy is the decrease in spatial resolution with increasing imaging depth. In lymph nodes using NIR excitation at a depth of 50 μm the axial resolution is already 2 to 5 times lower compared with the image quality obtained at the surface [14[•]]. Figure 5d shows that despite sufficient signal coming out of deep tissue regions, the resolution of cell borders and subcellular detail is strongly affected in scattering tumor tissue.

Figure 6



3D reconstruction of dendritic cells (DC) within a fixed lymph node. Syngeneic immature CMTR-positive DC were injected into the footpad of Balb/C mice 24 h before explantation of the draining popliteal lymph node, as described [10]. **(a)** Reconstruction at an excitation wavelength of 880 nm and **(b)** normalized red fluorescence as a function of penetration depth (measured as z-profile in the dashed regions). **(c)** Reconstruction at an excitation wavelength of 1100 nm. **(d)** Individual xy-sections in the deep T cell zone at depths of 400–700 μm. Excitation power was 110 mW (1100 nm) and 180 mW (880 nm). Bar, 100 μm.

However, our measurements indicate that this degradation is significantly reduced for IR-MPM compared with NIR-MPM (V Andresen, P Friedl, unpublished data). Thus, for a certain depth window IR-MPM delivers images of unrivaled quality.

Conclusions

These findings establish infrared two-photon and second harmonic generation microscopy for non-toxic time-resolved investigation of cell behavior with particular benefit for deep tissue imaging. As being advantageous compared with other pulsed femtosecond IR laser systems, including Ch:forsterite (1230 nm) and Fianium fiber (1064 nm) lasers, the wavelength generated by the OPO is tuneable and thus suited to excite red and NIR fluorophores in a flexible manner at their excitation peaks. Without a major compromise in resolution, the wavelength range of 1100 to 1300 nm is well suited for two-photon excitation of red and NIR fluorophores, as well as genetically encoded red-shifted fluorescent proteins (DsRed2, mCherry, TurboFP) and broad-band

SHG, yet it spares restrictive water absorption enabling approximately doubled penetration of interstitial tissues and cell-rich compartments compared with NIR excitation.

Future developments to enhance IR-MPM will include the creation of further red-shifted genetically encoded fluorescent proteins; IR-excited fluorescence lifetime imaging (FLIM) studies for discriminating multiple fluorophores with similar emission spectra [26]; the combination with optical coherence tomography in order to pre-select regions of interest [27]; and the implementation of adaptive optics [28^{••}]. The latter is of particular importance for deep imaging in tissue as local changes in the refractive index caused by cell membranes, fat deposits, and the like degrade the excitation wavefront and thus the PSF significantly [29]. In two-photon microscopy this, in turn, does not only lead to a reduction in image quality but also to a considerable loss of fluorescence as signal depends on the square of the laser power. Using adaptive optics and a single correction shape for a given depth

8 Analytical biotechnology

should enable to compensate for 80% of the sample-induced aberrations [30].

IR-multiphoton microscopy will be useful for imaging cell and tissue structures in native state, using third harmonic generation (THG) and OPO-excited CARS. Third harmonic generation (THG) is a nonlinear optical microscopic technique that, similar to SHG, is caused by third-order nonlinear processes [20]. As it depends nonlinearly on the excitation power THG features inherent optical sectioning. Its nonresonant nature in combination with NIR excitation wavelengths (1–2 μm) renders this technique very interesting for imaging biological and non-biological specimens [31].

Using a Nd:vanadate or Ti:Sa laser in combination with a synchronously pumped OPO will further allow CARS as a powerful tool for imaging cells and tissues in native state [32]. Thereby, the Ti:Sa radiation acts as pump beam and the OPO radiation as Stokes beam for the CARS nonlinear process, suited for studies of lipid metabolism or organelle transport in live cells.

Simultaneous multiphoton measurements of green and red fluorophores will benefit from recent advances in Ti:Sa and OPO development. The latest Ti:Sa laser generation features output powers above 4 W enabling the use of several 100 mW for both excitation beams. Lastly, a new generation of OPO crystals will allow tuning of the pump beam wavelength over a broad area and thus support simultaneous excitation of green and red fluorophores at their respective excitation peaks. In conclusion, the common insight ‘redder is better’ holds true for deep tissue two-photon microscopy with implications for a broad range of applications in biomedical research.

Acknowledgements

We gratefully acknowledge Thorsten Mempel and Ulrich von Andrian for providing lymph node samples and Monika Kuhn for expert technical assistance. This work was supported by the DFG (grant number FR1155/8-1) and the EU network of excellence EMIL (LSHC-CT-2004-503569) to PF and the National Institutes of Health grant CA103563 to RMH.

References and recommended reading

Papers of particular interest, published within the period of review, have been highlighted as:

- of special interest
- of outstanding interest

1. Condeelis J, Segall JE: **Intravital imaging of cell movement in tumours.** *Nat Rev Cancer* 2003, **3**:921-930.
 2. Helmchen F, Denk W: **Deep tissue two-photon microscopy.** *Nat Methods* 2005, **2**:932-940.
 3. Crepel V, Aronov D, Jorquera I, Represa A, Ben-Ari Y, Cossart R: **A parturition-associated nonsynaptic coherent activity pattern in the developing hippocampus.** *Neuron* 2007, **54**:105-120.
 4. Theer P, Hasan MT, Denk W: **Two-photon imaging to a depth of 1000 μm in living brains by use of a Ti:Al₂O₃ regenerative amplifier.** *Opt Lett* 2003, **28**:1022-1024.
 5. Denk W, Strickler JH, Webb WW: **Two-photon laser scanning fluorescence microscopy.** *Science* 1990, **248**:73-76.
 6. Friedl P, Wolf K, von Andrian UH, Harms G: **Biological second and third harmonic generation microscopy.** *Curr Protoc Cell Biol* 2004, **15**:1-21.
 7. Zoumi A, Yeh A, Tromberg BJ: **Imaging cells and extracellular matrix *in vivo* by using second-harmonic generation and two-photon excited fluorescence.** *Proc Natl Acad Sci U S A* 2002, **99**:11014-11019.
 8. Zipfel WR, Williams RM, Christie R, Nikitin AY, Hyman BT, Webb WW: **Live tissue intrinsic emission microscopy using multiphoton-excited native fluorescence and second harmonic generation.** *Proc Natl Acad Sci U S A* 2003, **100**:7075-7080.
 9. Masters BR, So PT, Gratton E: **Multiphoton excitation fluorescence microscopy and spectroscopy of *in vivo* human skin.** *Biophys J* 1997, **72**:2405-2412.
 10. Mempel TR, Henrickson SE, Von Andrian UH: **T-cell priming by dendritic cells in lymph nodes occurs in three distinct phases.** *Nature* 2004, **427**:154-159.
 11. Rothstein EC, Carroll S, Combs CA, Jobsis PD, Balaban RS: **Skeletal muscle NAD(P)H 2-photon fluorescence microscopy *in vivo*: topology and optical inner filters.** *Biophys J* 2005, **88**:2165-2176.
 12. Dunn KW, Sandoval RM, Kelly KJ, Dagher PC, Tanner GA, Atkinson SJ, Bacallao RL, Molitoris BA: **Functional studies of the kidney of living animals using multicolor 2-photon microscopy.** *Am J Physiol Cell Physiol* 2002, **283**: C905-916.
 13. Brown EB, Campbell RB, Tsuzuki Y, Xu L, Carmeliet P, Fukumura D, Jain RK: ***In vivo* measurement of gene expression, angiogenesis and physiological function in tumors using multiphoton laser scanning microscopy.** *Nat Med* 2001, **7**:864-868.
 14. Niesner RA, Andresen V, Neumann J, Spiecker H, Gunzer M: **The power of single- and multibeam 2-photon microscopy for high-resolution and high-speed deep tissue and intravital imaging.** *Biophys J* 2007.
- Rigorous study of principles, performances and limitations of single-beam and multi-beam 2-photon microscopy for tissue imaging.
15. Yamamoto N, Jiang P, Yang M, Xu M, Yamauchi K, Tsuchiya H, Tomita K, Wahl GM, Moossa AR, Hoffman RM: **Cellular dynamics visualized in live cells *in vitro* and *in vivo* by differential dual-color nuclear-cytoplasmic fluorescent-protein expression.** *Cancer Res* 2004, **64**:4251-4256.
 16. Hopt A, Neher E: **Highly nonlinear photodamage in two-photon fluorescence microscopy.** *Biophys J* 2001, **80**:2029-2036.
- Explores the relation between excitation intensity and photodamage for 2-photon imaging of bovine adrenal chromaffin cells.
17. Koenig K: **Multiphoton microscopy in life sciences.** *J Microsc* 2000, **200**:83-104.
 18. Dashkevich VI, Bui AA, Lisinetskii VA, Shkadarevich AP, Chulkov RV, Orlovich VA: **Tunable optical parametric oscillator based on a KTP crystal, pumped by a pulsed Ti³⁺:Al₂O₃ laser.** *J Appl Spectr* 2007, **74**:390-395.
 19. Torok P, Kao FJ: **Point-spread function reconstruction in high aperture lenses focusing ultra-short laser pulses.** *Opt Comm* 2002, **213**:97-102.
 20. Barad Y, Eisenberg H, Horowitz M, Silberberg Y: **Nonlinear scanning laser microscopy by third harmonic generation.** *Appl Phys Lett* 1997, **70**:922-924.
 21. Dickinson ME, Simbuerger E, Zimmermann B, Waters CW, Fraser SE: **Multiphoton excitation spectra in biological samples.** *J Biomed Opt* 2003, **8**:329-338.
 22. Eggeling C, Volkmer A, Seidel CA: **Molecular photobleaching kinetics of Rhodamine 6G by one- and two-photon induced confocal fluorescence microscopy.** *Chemphyschem* 2005, **6**:791-804.
- Presents strategies to determine fluorophore photobleaching and to quantify photokinetic parameters that describe the dependency of fluorescence signal and excitation irradiance.

23. Haleand G, Query M: **Optical constants of water in the 200-nm to 200- μ m wavelength region.** *Appl Opt* 1973, **12**:555-563.
24. Muller M, Squier J, Wilson KR, Brakenhoff GJ: **3D microscopy of transparent objects using third-harmonic generation.** *J Microsc* 1998, **191**:266-274.
25. Alexander S, Koehl GE, Hirschberg M, Geissler EK, Friedl P: **Dynamic imaging of cancer growth and invasion: a modified skin-fold chamber model.** *Histochem Cell Biol* 2008, **130**:1147-1154.
26. Koenig K, Riemann I: **High-resolution multiphoton tomography of human skin with subcellular spatial resolution and picosecond time resolution.** *J Biomed Opt* 2003, **8**:432-439.
27. Huang D, Swanson EA, Lin CP, Schuman JS, Stinson WG, Chang W, Hee MR, Flotte T, Gregory K, Puliafito CA: **Optical coherence tomography.** *Science* 1991, **254**:1178-1181.
28. Rueckel M, Mack-Bucher JA, Denk W: **Adaptive wavefront correction in two-photon microscopy using coherence-gated wavefront sensing.** *Proc Natl Acad Sci U S A* 2006, **103**:17137-17142.
Demonstrates spatial resolution and signal intensity improvement in 2-photon microscopy through adaptive correction of microscope and specimen induced wavefront aberrations.
29. Schwertner M, Booth MJ, Wilson T: **Measurement of optical aberrations induced in biological samples.** *Opt Express* 2004, **12**:6540-6552.
30. Marsh PN, Burns D, Girkin JM: **Practical implementation of adaptive optics in multiphoton microscopy.** *Opt Express* 2003, **11**:1123-1130.
31. Müller M, Squier J, Wilson KR, Brakenhoff GJ: **3D microscopy of transparent objects using third-harmonic generation.** *J Microsc* 1998, **191**:266-274.
32. Evans CL, Potma EO, Puoris'haag M, Cote D, Lin CP, Xie XS: **Chemical imaging of tissue *in vivo* with video-rate coherent anti-Stokes Raman scattering microscopy.** *PNAS* 2005, **102**:16807-16812.